Fountain Journal of Basic Medical and Health Sciences (FUJBMHES), 2(1), **122-139**

Corosolic Acid Attenuates Cognitive Deficits, Oxidative Stress, Neuroinflammation and Corticohippocampal Neurodegeneration in D-galactose-Induced Alzheimer's Disease in Adult Wistar Rats

Adunfe, O. O.[1,2]*, Abayomi, T. A.[2], Tokunbo, O. S.[2], Olayemi, O. S.[2], Oguntade, A. A.[1], Farinde, R. A.[1], Oyadare, O. S.[2], & Dare, B. J.[2]

[1]Anatomy Unit, Department of Medical Laboratory Science, Fountain University, Osogbo.
[2]Department of Anatomy, Faculty of Basic Medical Sciences, College of Health Sciences, Osun State University, Osogbo, Nigeria.

**Corresponding author: adunfe.oluwatobi@fuo.edu.ng; +2348160645738*

Abstract

Background: Alzheimer's disease is characterised by progressive corticohippocampal dysfunction driven by oxidative stress, neuroinflammation and cholinergic decline. Corosolic acid, a pentacyclic triterpenoid, possesses antioxidant and anti-inflammatory activity, but its effect on the corticohippocampal axis in a chronic ageing model is unknown. This study evaluated the neuroprotective effect of corosolic acid, relative to donepezil, in D-galactose-induced neurotoxicity in adult male Wistar rats. **Methodology:** Rats were exposed to D-galactose (120 mg/kg/day, orally, 42 days) and treated with corosolic acid or the reference drug donepezil. Learning and memory were assessed by the Morris water maze, Y-maze spontaneous alternation and novel object recognition tests. Superoxide dismutase (SOD) activity, nuclear factor kappa B (NF-κB) and acetylcholinesterase (AChE) were quantified in the prefrontal cortex and hippocampus. Neuronal and neurofibrillary architecture was examined by haematoxylin and eosin (H&E) and Bielschowsky silver staining. **Results:** D-galactose significantly impaired performance across all three behavioural paradigms, reduced SOD activity, elevated NF-κB and AChE, and produced marked neuronal degeneration and neurofibrillary fragmentation in the prefrontal cortex and hippocampal CA3 ($p < 0.05$). Corosolic acid significantly reversed each of these changes, restoring escape latency, spontaneous alternation and novel-object exploration toward control values, normalising SOD, NF-κB and AChE in both regions, and preserving neuronal and neurofibrillary integrity. On several endpoints — notably novel object recognition and cortical SOD activity — corosolic acid matched or exceeded the protection afforded by donepezil. **Conclusion:** Corosolic acid confers multi-domain neuroprotection against D-galactose-induced corticohippocampal injury, acting on oxidative, inflammatory, cholinergic, and structural endpoints, with efficacy comparable to or superior to that of donepezil on several measures. These findings identify corosolic acid as a promising candidate for further investigation in age-related neurodegeneration.

Keywords: Pentacyclic triterpenoid; brain ageing; antioxidant enzymes; acetylcholinesterase; hippocampus.

Introduction

Alzheimer's disease (AD) is the commonest cause of dementia worldwide and one of the defining public-health challenges of an ageing global population. It is a chronic, progressive neurodegenerative disorder characterised clinically by an insidious decline in episodic memory, followed by deterioration in language, executive function, visuospatial ability and, ultimately, the capacity for independent living (Scheltens et al., 2021). Current estimates place the number of people living with dementia at approximately 55

 ISSN: 1595-1693

million globally, a figure projected to rise to 78 million by 2030 and 139 million by 2050, with AD accounting for an estimated 60–70% of cases (GBD 2019 Dementia Forecasting Collaborators, 2022).

Critically for the present study, this burden is not evenly distributed. More than 60% of people living with dementia reside in low- and middle-income countries, and this proportion is projected to rise further as demographic transition accelerates across sub-Saharan Africa and South Asia (Sexton et al., 2021). These are precisely the settings in which access to disease-modifying immunotherapies is most constrained by cost, infrastructure and the requirement for specialist neuroimaging and genotyping. The search for affordable, orally bioavailable, plant-derived neuroprotective agents is therefore not merely of academic interest but of direct translational and equity relevance.

The neuropathological definition of AD rests upon two protein lesions: extracellular plaques of aggregated amyloid-beta (Aβ) peptide, generated by sequential β- and γ-secretase cleavage of the amyloid precursor protein, and intraneuronal neurofibrillary tangles composed of hyperphosphorylated, misfolded tau protein (Breijyeh and Karaman, 2020). The amyloid cascade hypothesis, which positions Aβ dysmetabolism as the upstream initiating event that drives downstream tau pathology, synaptic failure and neuronal death, has dominated the field for three decades and continues to frame therapeutic development (Beshir et al., 2024).

It is now widely accepted, however, that this binary account is insufficient. AD is more accurately conceptualised as a multifactorial disorder in which Aβ and tau pathology are embedded within, and amplified by, a network of interacting pathogenic processes: oxidative stress, mitochondrial dysfunction, chronic neuroinflammation, cholinergic deficit, disrupted calcium homeostasis, impaired autophagy and caspase-dependent neuronal apoptosis (Breijyeh and Karaman, 2020; d'Errico and Meyer-Luehmann, 2020).

The corticohippocampal axis — comprising the hippocampal formation and its reciprocally connected entorhinal and adjacent neocortical territories — constitutes the anatomical substrate of declarative memory encoding, consolidation and spatial navigation. It is also, notably, among the earliest and most severely affected regions in AD. Neurofibrillary pathology characteristically originates in the transentorhinal and entorhinal cortices before spreading to the hippocampus proper and thereafter to association neocortex, a topographical progression that correlates closely with the clinical evolution of cognitive impairment (Olajide et al., 2021).

Advancing age is the single greatest risk factor for AD, and experimental models that reproduce the biochemical features of brain ageing are therefore of considerable value. Chronic administration of D-galactose has become one of the most widely adopted models. At physiological concentrations, D-galactose is metabolised normally by galactokinase and galactose-1-phosphate uridyltransferase; when administered in excess, however, it saturates these pathways and is instead reduced to galactitol by aldose reductase or oxidised to aldehydes and hydrogen peroxide by galactose oxidase. The surplus reducing sugar undergoes non-enzymatic Maillard reaction with free amino groups of proteins to yield advanced glycation end-products (AGEs) (Zeng et al., 2021). Engagement of AGEs with their receptor (RAGE) activates NADPH oxidase and NF-κB signalling, generating a self-sustaining cycle of ROS production and pro-inflammatory cytokine release. A systematic review and meta-analysis of the D-galactose literature confirmed a robust and reproducible effect on cognitive outcomes and oxidative stress indices across a wide range of doses, durations, routes of administration, species and sexes, while also drawing attention to substantial heterogeneity between laboratories (Sadigh-Eteghad et al., 2017). The model has been successfully deployed to evaluate a range of candidate neuroprotectants within the corticohippocampal axis, including plant-derived oligosaccharides (Deng et al., 2020), coumarins

 ISSN: 1595-1693

(Wang et al., 2023), amino acid derivatives (Zeng et al., 2021) and flavonoids (Haider et al., 2020).

Plant-derived compounds have attracted sustained interest as candidate neurotherapeutics because they frequently act upon several pathogenic pathways simultaneously, are generally well tolerated, and are typically inexpensive and locally accessible. Pentacyclic triterpenoids — a class that includes ursolic, oleanolic, asiatic, betulinic and corosolic acids — are of particular interest. Their lipophilic character favours passage across the blood–brain barrier, and members of the class have been shown to activate Nrf2-mediated antioxidant defences, suppress NF-κB-driven inflammatory transcription, and attenuate apoptotic signalling in neural tissue.

Corosolic acid (2α,3β-dihydroxyurs-12-en-28-oic acid; $C_{30}H_{48}O_4$, molecular weight 472.70 g/mol) is an ursane-type pentacyclic triterpenoid isolated most abundantly from the leaves of *Lagerstroemia speciosa* (banaba), and additionally from *Prunus armeniaca*, *Eucalyptus globulus*, *Crataegus pinnatifida* and *Centella asiatica*. Widely designated "plant insulin" on account of its glucose-lowering activity, it is already marketed as a dietary supplement in several jurisdictions, which affords a useful preliminary indication of tolerability in humans.

Its documented pharmacological repertoire is broad and includes hypoglycaemic, anti-obesity, anti-neoplastic, hepatoprotective, cardioprotective, antioxidant and anti-inflammatory activities (Zhao et al., 2021).

The quest for disease-modifying interventions in neurodegeneration has, increasingly, turned to naturally occurring compounds, which target the multifactorial pathology of these disorders. Oxidative stress, neuroinflammation, mitochondrial dysfunction and cholinergic loss act in concert rather than isolation. Therefore, agents which can modulate several of these processes simultaneously are theoretically better suited to the problem than single target drugs, whose limited success in Alzheimer's disease is well documented (Breijyeh & Karaman, 2020). In this regard, dietary and medicinal phytochemicals are attractive as they are usually pleiotropic, are generally well tolerated for long periods and often can cross the blood–brain barrier due to their lipophilicity. Therefore, phytochemicals from different structural classes have been tested in the D-galactose model, with convergent results. Polyphenols and flavonoids such as the anthocyanins (Rehman et al., 2017), quercetin via Nrf2–ARE axis (Dong et al., 2017), the flavonoid naringenin (Haider et al., 2020) and more recently luteolin via SIRT1 signalling (Younis et al., 2024) have each been demonstrated to rescue learning and memory, restore antioxidant enzyme activity and suppress neuroinflammatory mediators. A similar pattern is seen for non-flavonoid agents. The methylxanthine caffeine (Ullah et al., 2015), the amino-acid derivative L-theanine on AGE formation and BDNF signalling (Zeng et al., 2021), the coumarin osthole (Wang et al., 2023) and the iridoid-rich extract OMO (Deng et al., 2020) all afford appreciable neuroprotection. This consistency across chemically diverse compounds supports the view that efficacy of phytochemicals against cognitive decline is underpinned by multi-target antioxidant and anti-inflammatory activity, rather than any single molecular interaction. In this respect, the corosolic acid is still poorly explored in the neurodegeneration literature. While the closely related analogue, ursolic acid, has been repeatedly shown to activate Nrf2 signalling and maintain mitochondrial function in models of ageing and amyloid toxicity, the evidence base for corosolic acid is dominated by its metabolic and oncological actions, with only isolated reports of direct neuroprotection, most notably against cerebral ischaemia–reperfusion injury (Zhang et al., 2022). The present study therefore fills a specific knowledge gap: whether the antioxidant and anti-inflammatory pharmacology observed by us for corosolic acid in peripheral tissues can be extended to the corticohippocampal axis in a chronic brain ageing model and if this protection is comparable to a clinically used cholinesterase inhibitor.

 ISSN: 1595-1693

Materials and Methods

Chemicals and Reagents

D-galactose (D-(+)-galactose; CAS No. 59-23-4; molecular formula $C_6H_{12}O_6$; molecular weight 180.16 g/mol) and corosolic acid (2α,3β-dihydroxyurs-12-en-28-oic acid; CAS No. 4547-24-4; molecular formula $C_{30}H_{48}O_4$; molecular weight 472.70 g/mol; purity ≥ 98% by HPLC) were procured from Atkins Chemicals. Donepezil (Standard drug) was procured from AKOL pharmacy in Osogbo. All other reagents used in this study were of analytical grade.

Assay kits were obtained from Elabscience Biotechnology Inc. (Wuhan, China) as follows: Total Superoxide Dismutase (T-SOD) Activity Assay Kit, WST-1 method (Catalogue No. E-BC-K020-M); Rat NF-κB p65 (Nuclear Factor Kappa B p65) ELISA Kit (Catalogue No. E-EL-R0674); and Rat AChE (Acetylcholinesterase) ELISA Kit (Catalogue No. E-EL-R0355). All kits were stored and handled strictly in accordance with the manufacturer's specifications and were used within their stated shelf life.

Experimental Animals and Husbandry

Forty-eight (48) adult male Wistar rats weighing approximately 155 ± 10 g were procured from the animal holding unit of the Faculty of Basic Medical Sciences, Osun State University, Osogbo, Nigeria. The animals were housed in standard plastic cages with softwood shavings as bedding at the central animal house of the College of Health Sciences, Osun State University, under conventional laboratory conditions (temperature 25 ± 2 °C, relative humidity 50–60%, and a 12-hour light/dark cycle). Rats were provided with standard rodent pellets and clean drinking water *ad libitum* throughout the study, and bedding was changed twice weekly. The animals were acclimatised to the housing environment for two weeks prior to the commencement of the experiment.

Ethical Approval

The study protocol was reviewed and approved by the Ethical Review Committee of the College of Health Sciences, Osun State University. All procedures were conducted in strict accordance with the National Institutes of Health *Guide for the Care and Use of Laboratory Animals* (8th edition) and are reported in conformity with the ARRIVE 2.0 guidelines. Every effort was made to minimise animal suffering and to employ the minimum number of animals consistent with statistical validity.

Experimental Design and Animal Grouping

Following acclimatisation, rats were randomly assigned into six groups of eight animals each (n = 8). Group allocation was concealed from the investigators responsible for behavioural scoring and for histological and biochemical analysis, all of whom remained blinded to treatment identity until data analysis was complete. The treatment schedule for all groups spanned six weeks (42 consecutive days).

Table 1. Experimental design, group allocation and treatment regimen.

Groups	**Treatment**	**Route and duration**
Control	Normal saline (0.9% NaCl), equivalent volume	Oral gavage; 42 days
D-gal	D-galactose (120 mg/kg/day)	Oral gavage; 42 days
Corosolic acid	Corosolic acid (10 mg/kg/day)	Oral gavage; 42 days
Donepezil	Donepezil (5 mg/kg/day)	Oral gavage; 42 days
D-gal + Corosolic acid	D-galactose (120 mg/kg/day) + Corosolic acid (10 mg/kg/day)	Oral gavage; 42 days
D-gal + Donepezil	D-galactose (120 mg/kg/day) + Donepezil (5 mg/kg/day)	Oral gavage; 42 days

ISSN: 1595-1693

Preparation and Administration of Test Substances

D-galactose was freshly dissolved in normal saline (0.9% NaCl) each morning to yield a concentration sufficient to administer 120 mg/kg body weight in a dosing volume not exceeding 10 mL/kg. Corosolic acid, being poorly water-soluble, was first dissolved in a minimal volume of dimethyl sulfoxide (DMSO) and subsequently diluted with 0.5% carboxymethylcellulose (CMC) in distilled water to produce a homogeneous suspension, with the final DMSO concentration maintained below 1% (v/v). Control animals received an equivalent volume of the vehicle.

All substances were administered once daily by oral gavage using a flexible stainless-steel or polypropylene gavage needle, between 08:00 and 10:00 hours, for 42 consecutive days. In the combination groups, corosolic acid and Donepezil were administered 60 minutes after the D-galactose dose in order to avoid any direct physicochemical interaction within the gastrointestinal lumen. Preparations were made fresh daily and protected from light.

Behavioural Assessment

Novel Object Recognition (NOR) Test

Non-spatial recognition memory was assessed in the novel object recognition test, performed as previously described (Tropea et al., 2022). The novel object recognition test exploits the innate preference of rodents for novelty and provides an index of non-spatial recognition memory that is dependent upon the perirhinal cortex and hippocampus. Testing was conducted in an open-field arena measuring 60 × 60 × 40 cm constructed of opaque material, and comprised three phases. On day 43, each rat was placed individually in the empty arena and permitted to explore freely for 10 minutes to reduce neophobia and locomotor exploration attributable to the arena itself. On day 44, two identical objects (A_1 and A_2) of equal size, colour and texture were placed in diagonally opposite quadrants, approximately 10 cm from the arena walls. Each rat was introduced, facing away from both objects, and given 10 minutes of free exploration.

After an inter-trial interval of one hour, one familiar object was replaced with a novel object (B) differing in shape, colour and texture but comparable in size and height, and the animal was returned to the arena for 5 minutes. The position of the novel object was counterbalanced across animals within each group to control for side preference, and objects were of sufficient weight that they could not be displaced. Exploration was operationally defined as directing the nose toward an object at a distance of ≤ 2 cm, or touching the object with the nose or vibrissae; climbing upon or sitting on an object without directed sniffing was not scored as exploration. The arena and objects were cleaned thoroughly with 70% ethanol and dried between every animal to eliminate residual olfactory cues. Sessions were video-recorded and scored by an observer blinded to group allocation. The following indices were derived, where T_N and T_F denote time spent exploring the novel and familiar objects respectively:

Discrimination Index (DI) = $(T_N - T_F) / (T_N + T_F)$

Recognition Index (RI, %) = $[T_N / (T_N + T_F)] \times 100$

Animals exploring for less than 20 seconds during the retention phase were excluded from analysis, in accordance with standard practice.

Y-Maze Spontaneous Alternation Test

Spatial working memory was evaluated using the Y-maze spontaneous alternation test, conducted as described by Kraeuter, Guest and Sarnyai (2019). Spontaneous alternation behaviour in the Y-maze reflects hippocampus-dependent spatial working memory and the innate tendency of rodents to explore a previously unvisited arm. The apparatus consisted of three identical opaque arms (A, B and C), each 50 cm long × 15 cm wide with 30 cm high walls, radiating from a central triangular platform at 120° to one another.

On day 43, each rat was placed at the distal end of one arm facing the centre and allowed to explore the maze freely for 8 minutes. The sequence and total number of arm entries were recorded; an

 ISSN: 1595-1693

entry was scored only when all four paws had crossed into an arm. A spontaneous alternation was defined as consecutive entry into all three different arms in overlapping triplet sets (for example, the sequence ABCACB contains four alternations). The percentage of spontaneous alternation was calculated as:

Alternation (%) = [Number of alternations / (Total arm entries − 2)] × 100

The total number of arm entries was recorded separately as an index of general locomotor and exploratory activity, permitting any group difference in alternation to be interpreted independently of gross motor impairment. The maze was cleaned with 70% ethanol and permitted to dry between animals.

Morris Water Maze (MWM)

Hippocampus-dependent spatial learning and reference memory were assessed in the Morris water maze, performed as previously described (Haider et al., 2020). The Morris water maze was employed to assess hippocampus-dependent spatial learning and reference memory. The apparatus comprised a circular pool 150 cm in diameter and 60 cm deep, filled to a depth of 35 cm with water maintained at 22 ± 1 °C and rendered opaque by the addition of powdered skimmed milk. The pool was notionally divided into four equal quadrants (north-east, north-west, south-east and south-west), and a circular escape platform 10 cm in diameter was submerged 1.5 cm below the water surface at the centre of the target (north-west) quadrant. Prominent distal visual cues of differing geometric shape and colour were affixed to the surrounding walls and remained unchanged for the duration of testing.

Over four consecutive days (days 44–47), each rat received four trials per day with an inter-trial interval of 20 minutes. At the start of each trial the animal was gently released into the water facing the pool wall from one of the four quadrants, the order of release points being pseudorandomised across trials and days such that no animal was released from the same quadrant twice in succession. Each trial terminated when the rat located and mounted the platform, or after a maximum of 60 seconds. A rat failing to locate the platform within 60 seconds was gently guided to it and assigned a latency of 60 seconds. All animals were permitted to remain on the platform for 20 seconds at the end of each trial to consolidate the spatial cue relationship, then dried and returned to a warmed holding cage. Escape latency and swim path length were recorded.

Twenty-four hours after the final acquisition trial (day 48), the platform was removed and each rat was released from the quadrant diametrically opposite the former platform location and allowed to swim freely for 60 seconds. The time spent in the target quadrant, the number of crossings over the former platform site, and the latency to first entry into the target quadrant were recorded as indices of spatial reference memory retention. Swim speed was recorded throughout as a control for sensorimotor or motivational confounds. All trials were video-recorded from an overhead camera and analysed using video-tracking software by an observer blinded to group allocation. The water was stirred between animals to disperse olfactory cues and was changed daily.

Euthanasia and Tissue Collection

Twenty-four hours after the final behavioural test (day 49), animals were fasted overnight, weighed, and anaesthetised by intraperitoneal injection of ketamine (75 mg/kg) and xylazine (10 mg/kg). Following confirmation of loss of the pedal withdrawal reflex, blood was collected by cardiac puncture, and the animals were euthanised by decapitation. The brains were rapidly excised, rinsed in ice-cold phosphate-buffered saline (PBS, 0.01 M, pH 7.4), blotted, weighed, and divided along the midsagittal plane.

The left hemisphere of each animal was immersion-fixed in 10% neutral buffered formalin for histological and histochemical processing. From the right hemisphere, the cerebral cortex and hippocampus were carefully dissected free on an ice-cold glass plate, immersed in phosphate-buffered saline solution and stored at −80 °C pending biochemical analysis. This hemispheric division permitted both structural and

 ISSN: 1595-1693

biochemical endpoints to be obtained from every animal, thereby maximising statistical power without increasing animal numbers.

Biochemical Analyses

Preparation of Tissue Homogenates

Frozen cortical and hippocampal tissues were weighed and homogenised separately in ice-cold PBS (0.01 M, pH 7.4) containing a protease inhibitor cocktail, at a ratio of 1:9 (w/v) to yield a 10% homogenate. Homogenisation was performed on ice using a motor-driven Teflon-glass homogeniser, with care taken to avoid heat generation. Homogenates were centrifuged at 5,000 × *g* for 10 minutes at 4 °C, and the clear supernatant was aspirated, aliquoted and used for assay. Total protein concentration in each supernatant was determined by the Bradford method using bovine serum albumin as standard, to permit normalisation of all analyte concentrations to protein content. Samples were assayed in duplicate and repeated freeze–thaw cycles were avoided.

Superoxide Dismutase (SOD) Activity — Colorimetric Assay

Total superoxide dismutase activity was determined colorimetrically using the Elabscience Total Superoxide Dismutase (T-SOD) Activity Assay Kit (WST-1 method; Catalogue No. E-BC-K020-M), strictly in accordance with the manufacturer's protocol. In brief, 20 µL of sample supernatant was added to the appropriate wells, followed by the working reagents prepared as directed (Reagents 1 and 2 combined at a ratio of 200:1; Reagents 3 and 4 combined at a ratio of 1:10 on ice), giving a total reaction volume of 240 µL. Plates were mixed thoroughly and incubated at 37 °C for 30 minutes, after which absorbance was read at 450 nm using a microplate reader. Blank, control and sample wells were run in parallel. The assay has an analytical sensitivity of 0.2 U/mL and a detection range of 0.2–14.4 U/mL. Superoxide dismutase activity was expressed as units per milligram of total protein (U/mg protein).

Nuclear Factor Kappa B p65 (NF-κB p65)

Cortical and hippocampal NF-κB p65 concentrations were quantified using the Elabscience Rat NF-κB p65 ELISA Kit (Catalogue No. E-EL-R0674), a sandwich enzyme immunoassay, following the manufacturer's instructions. The micro-ELISA plate supplied with the kit is pre-coated with an antibody specific to rat NF-κB p65.

One hundred microlitres of standard or sample supernatant was added to each well and incubated for 90 minutes at 37 °C. The liquid was decanted and 100 µL of biotinylated detection antibody working solution added to each well, followed by incubation for 60 minutes at 37 °C. After three washes, 100 µL of horseradish peroxidase (HRP)–avidin conjugate working solution was added and the plate incubated for a further 30 minutes at 37 °C. Following five washes, 90 µL of tetramethylbenzidine (TMB) substrate solution was added to each well and the plate incubated in the dark at 37 °C for approximately 15 minutes, whereupon wells containing the analyte developed a blue colouration. The reaction was terminated by the addition of 50 µL of stop solution, producing a colour change to yellow, and the optical density of each well was read immediately at 450 ± 2 nm. Analyte concentrations were interpolated from a four-parameter logistic standard curve constructed from the kit standards and expressed as nanograms per milligram of protein.

Acetylcholinesterase (AChE)

Acetylcholinesterase concentration in cortical and hippocampal homogenates was determined using the Elabscience Rat AChE ELISA Kit (Catalogue No. E-EL-R0355), also a sandwich enzyme immunoassay employing a plate pre-coated with an antibody specific to rat AChE. The assay procedure, incubation times and wash steps were as described in the determination of *NF-κB p65*, with absorbance likewise read at 450 ± 2 nm. The kit has a detection range of 0.78–50 ng/mL and a sensitivity of 0.47 ng/mL, and no significant cross-reactivity or interference between rat AChE and its analogues has been reported by the

 ISSN: 1595-1693

manufacturer. Results were interpolated from the standard curve and expressed as nanograms per milligram of protein.

Histological and Histochemical Procedures

Tissue Processing

Formalin-fixed hemispheres were fixed for a minimum of 48 hours, then trimmed to isolate blocks containing the cerebral cortex and the dorsal hippocampus. Tissues were dehydrated through an ascending series of ethanol (70%, 80%, 95% and two changes of absolute ethanol), cleared in two changes of xylene, infiltrated with molten paraffin wax and embedded. Coronal sections of 5 µm thickness were cut on a rotary microtome, floated on a warm water bath, mounted on clean glass slides (poly-L-lysine-coated for silver impregnation), and dried overnight at 37 °C. Serial sections were collected so that adjacent sections could be stained by the two different methods described below, permitting direct comparison of the same anatomical field.

Haematoxylin and Eosin (H&E) Staining

Sections were dewaxed in two changes of xylene and rehydrated through descending grades of ethanol to distilled water. They were stained in Harris haematoxylin for 5–10 minutes, rinsed in running tap water, differentiated briefly in 1% acid alcohol, and blued in Scott's tap water substitute (or dilute ammonia water) until the nuclei appeared crisp blue. Sections were counterstained in 1% aqueous eosin for 1–2 minutes, rinsed, dehydrated through ascending ethanol, cleared in xylene, and mounted in DPX under a coverslip.

Bielschowsky Silver Impregnation

Adjacent sections were stained by the Bielschowsky silver impregnation technique to demonstrate axons, neurofibrils, neurofibrillary tangles and neuritic plaques, which are not resolved by routine H&E staining. Sections were dewaxed, rehydrated to distilled water and washed thoroughly in several changes of distilled water to remove all traces of ions that might interfere with silver deposition.

Sections were then placed in 10–20% aqueous silver nitrate solution and incubated in the dark at 37 °C for 15–30 minutes, after which they were rinsed in several changes of distilled water. Ammoniacal silver solution was freshly prepared by adding concentrated ammonium hydroxide dropwise to the silver nitrate solution, with continuous agitation, until the brown precipitate initially formed had just redissolved to yield a clear solution. Sections were transferred to this ammoniacal silver solution and incubated in the dark at 37 °C for approximately 30 minutes. Development was then effected by adding a few drops of developer solution (containing formalin, citric acid and nitric acid) to the ammoniacal silver bath, with the sections monitored continuously under the microscope until the neurofibrils and axons appeared sharply black against a pale background — typically within 1–5 minutes.

Development was arrested by rinsing in distilled water. Sections were toned in 0.2% aqueous gold chloride for 3–5 minutes where a cooler, more permanent tone was desired, rinsed, fixed in 5% aqueous sodium thiosulphate for 5 minutes, and washed thoroughly in running water. They were finally dehydrated through ascending ethanol, cleared in xylene and mounted in DPX.

Photomicrography and Morphometric Analysis

Representative fields were photographed using a digital camera mounted on a light microscope, with identical illumination and white-balance settings maintained across all groups.

Statistical Analysis

Data were analysed using GraphPad Prism version 9 are presented as mean ± standard error of the mean (SEM). Behavioural indices and biochemical concentrations were evaluated by one-way analysis of variance (ANOVA) followed by Tukey's honestly significant difference post-hoc test for pairwise comparison. A probability

 ISSN: 1595-1693

value of $p < 0.05$ was accepted as statistically significant throughout.

Results

Effects of Corosolic Acid on Behavioral Performance in D-galactose-Induced Cognitive Impairment

In the Morris water maze (Figure 1A), D-galactose markedly prolonged escape latency (72.32 ± 2.31 s) relative to control (33.41 ± 1.46 s, $p < 0.05$). Corosolic acid reduced latency to near-control values (36.06 ± 2.11 s, $p < 0.05$ vs D-gal), as did donepezil (39.63 ± 2.05 s, $p < 0.05$). In the Y-maze (Figure 1B), D-galactose lowered spontaneous alternation (55.17 ± 1.35%) versus control (69.63 ± 1.06%, $p < 0.05$); both corosolic acid (67.28 ± 1.51%) and donepezil (65.31 ± 0.93%) significantly improved alternation ($p < 0.05$). In the novel object recognition test (Figure 1C), novel-object exploration time fell in D-galactose rats (50.07 ± 1.03 s) relative to control (160.17 ± 1.35 s, $p < 0.05$); corosolic acid restored exploratory preference (157.83 ± 1.40 s, $p < 0.05$ vs D-gal), whereas the donepezil value (57.49 ± 1.72 s) remained close to that of the D-galactose group.

Effect of Corosolic Acid on Superoxide Dismutase (SOD) Activity in the Prefrontal Cortex and Hippocampus of D-galactose-Treated Wistar Rats

In the prefrontal cortex (Figure 2), D-galactose reduced SOD activity (0.53 ± 1.26 U/mg protein) relative to control (1.31 ± 1.34 U/mg protein, $p < 0.05$); corosolic acid restored activity (1.29 ± 1.43 U/mg protein, $p < 0.05$ vs D-gal), exceeding the donepezil value (0.69 ± 1.37 U/mg protein, $p < 0.05$ vs D-gal). In the hippocampus, D-galactose likewise lowered SOD activity (0.5 ± 1.42 U/mg protein) versus control (2.35 ± 1.61 U/mg protein, $p < 0.05$), and both corosolic acid (2.01 ± 1.22 U/mg protein) and donepezil (2.00 ± 1.24 U/mg protein) restored activity toward control ($p < 0.05$).

CA treatment mitigated against Neuroinflammatory Cascades in the Corticohippocampal regions following D-galactose Exposure

In the prefrontal cortex (Figure 3), D-galactose upregulated NF-κB (3.2 ± 1.94) relative to control (1.21 ± 0.33, $p < 0.05$); corosolic acid (1.26 ± 0.41) and donepezil (1.23 ± 0.37) both significantly reduced expression ($p < 0.05$ vs D-gal). The same pattern was seen in the hippocampus, where D-galactose elevated NF-κB (4.12 ± 2.08) versus control (1.26 ± 0.29, $p < 0.05$), with reductions following corosolic acid (1.29 ± 0.51) and donepezil (1.33 ± 0.14, $p < 0.05$ vs D-gal).

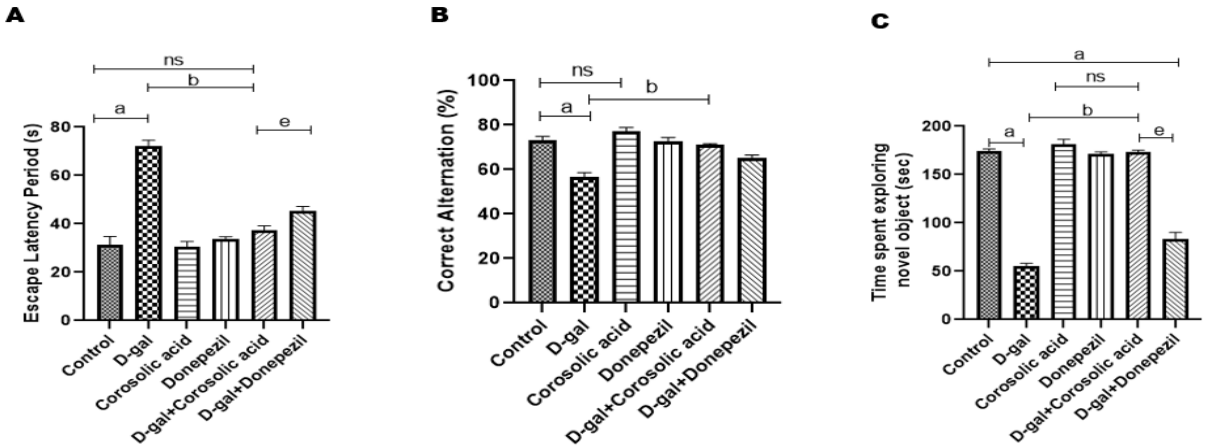

Figure 1: Effects of Corosolic acid on behavioural parameters in D-galactose-induced neurotoxicity**.** (A) Escape Latency Period in the Morris water maze test, (B) Percentage Correct

 ISSN: 1595-1693

Alternation in the Y-maze test, and (C) Time spent exploring a novel object in the Novel Object Recognition test. Data are expressed as Mean ± SEM. Letter variations indicate statistical significance ($p < 0.05$): a vs. Control; b vs. D-gal; e vs. D-gal+Corosolic acid; ns: non-significant.

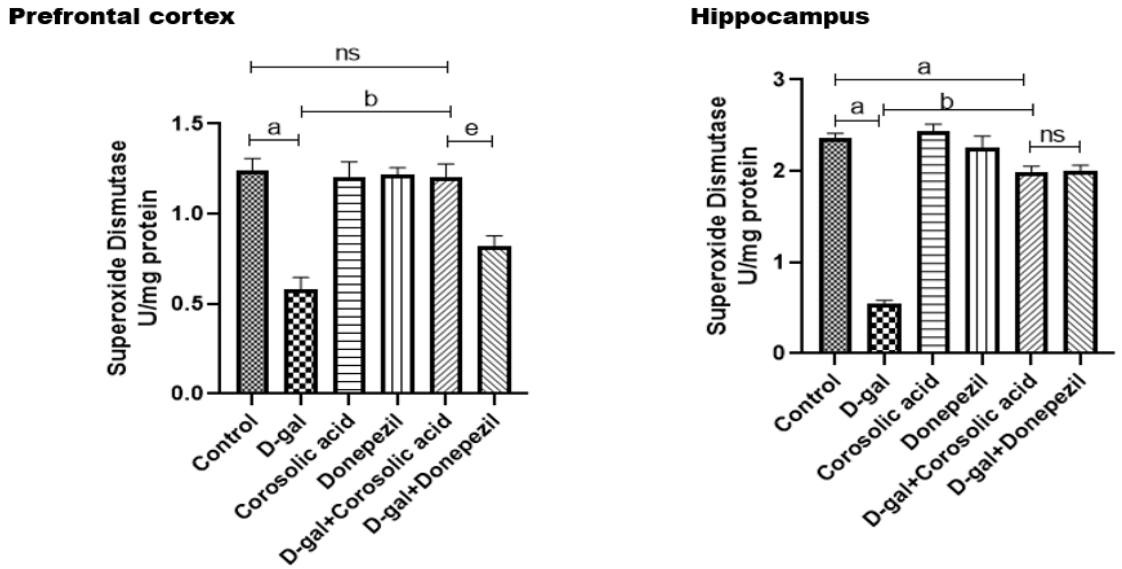

Figure 2: Modulation of Superoxide Dismutase (SOD) enzyme activity by Corosolic acid. Measurement of SOD activity in the prefrontal cortex and hippocampus. Bars represent Mean ± SEM. Significances ($p < 0.05$): Letter variations indicate statistical significance ($p < 0.05$): a vs. Control; b vs. D-gal; e vs. D-gal+Corosolic acid; ns: non-significant.

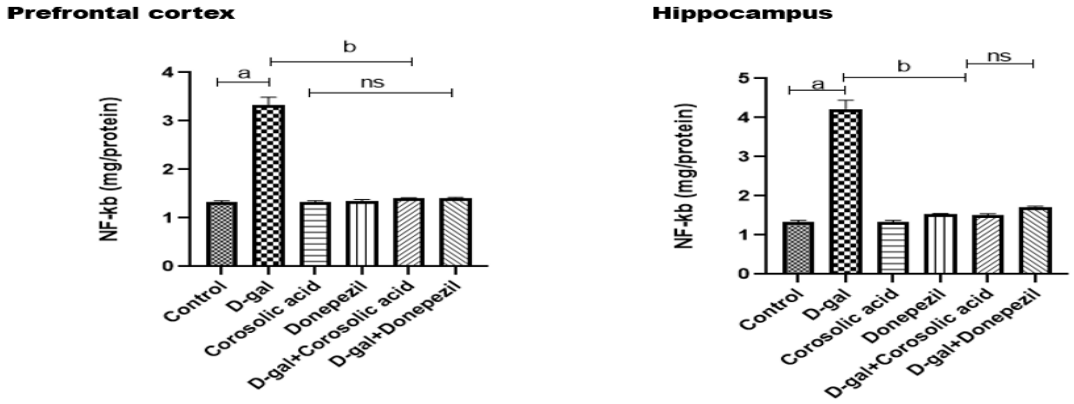

Figure 3: Influence of Corosolic acid on Nuclear Factor-kappa B (NF-κB) protein expression**.** Concentration of NF-κB in the prefrontal cortex and hippocampus. Bars represent Mean ± SEM. Significance ($p < 0.05$): Letter variations indicate statistical significance ($p < 0.05$): a vs Control; b vs D-gal; e vs D-gal+Corosolic acid; ns: non-significant.

Effect of Corosolic Acid on Acetylcholinesterase (AChE) Activity in the Prefrontal Cortex and Hippocampus of D-galactose-Treated Wistar Rats

 ISSN: 1595-1693

In the prefrontal cortex (Figure 4), D-galactose increased AChE activity (41.73 ± 0.88) relative to control (28.93 ± 0.93, $p < 0.05$); corosolic acid suppressed it to 30.03 ± 0.83 ($p < 0.05$ vs D-gal). In the hippocampus, AChE rose from a control value of 33.83 ± 1.51 to 47.82 ± 1.76 with D-galactose, and was reduced by corosolic acid (33.97 ± 1.42) and by donepezil (34.01 ± 1.39), both $p < 0.05$ versus D-galactose.

Histological Assessment of the Prefrontal Cortex and Hippocampus (H&E Stain) in D-galactose-Treated Wistar Rats Following Corosolic Acid Administration

Control sections showed normal cortical and CA3 cytoarchitecture with intact pyramidal neurons (Figures 5 and 6). D-galactose produced neuronal degeneration — cellular shrinkage, cytoplasmic vacuolation, pyknotic nuclei and disorganised cell layers — in both regions. Corosolic acid preserved neuronal morphology comparable to control, whereas the donepezil group showed partial restoration with some residual shrinkage and pyknosis.

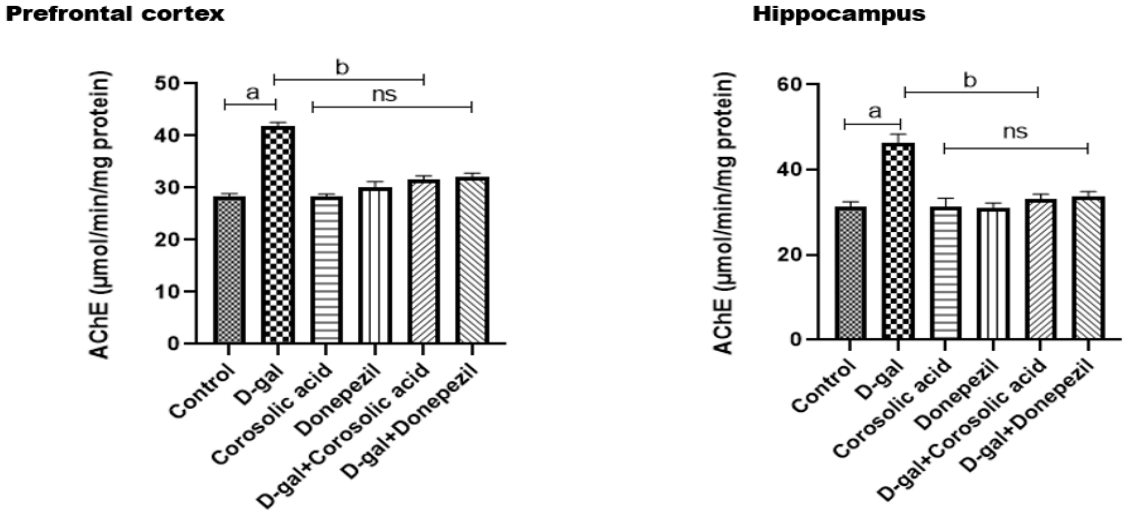

Figure 4: Regulatory effects of Corosolic acid on Acetylcholinesterase (AChE) enzyme activity**.** AChE enzyme kinetics in the prefrontal cortex and hippocampus. Bars represent Mean ± SEM. Significance ($p < 0.05$): Letter variations indicate statistical significance ($p < 0.05$): a vs Control; b vs D-gal; e vs D-gal+Corosolic acid; ns: non-significant.

 ISSN: 1595-1693

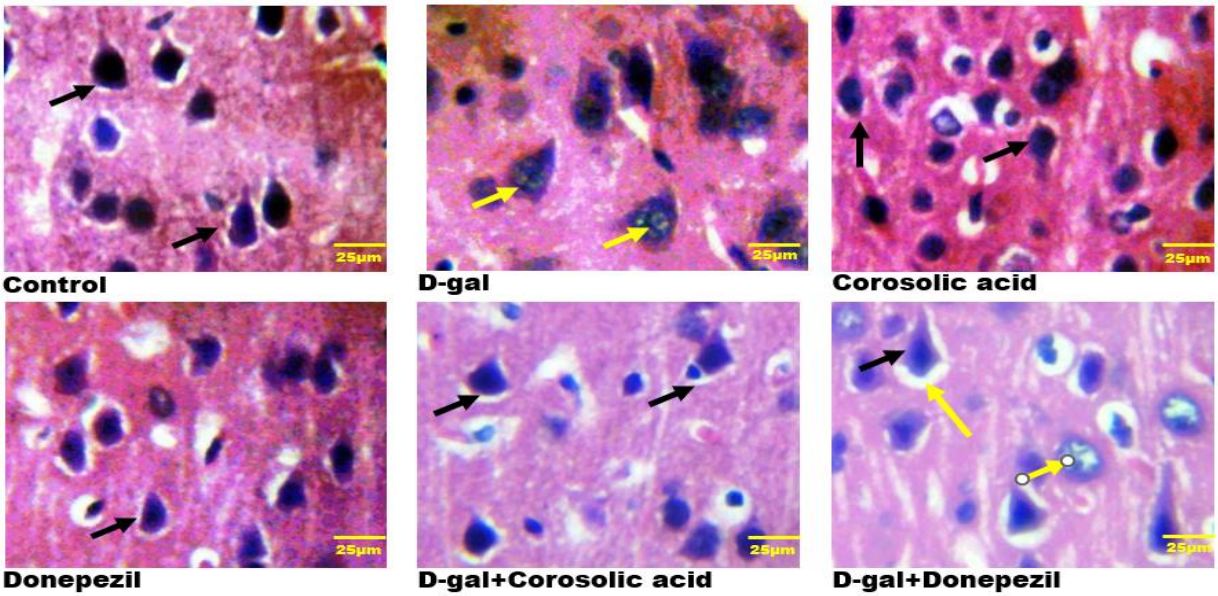

Figure 5: Photomicrographs of the prefrontal cortex stained with Hematoxylin and Eosin (H&E). Scale bar = 25µm. Black arrows show normal intact neurons; yellow arrows point to degenerating, pyknotic neurons. Control cortex shows abundant intact pyramidal neurons, whereas the D-galactose group shows widespread neuronal shrinkage, pyknosis and cytoplasmic vacuolation; corosolic acid preserves cortical cytoarchitecture to a degree comparable with control, while donepezil affords only partial protection with residual pyknotic profiles.

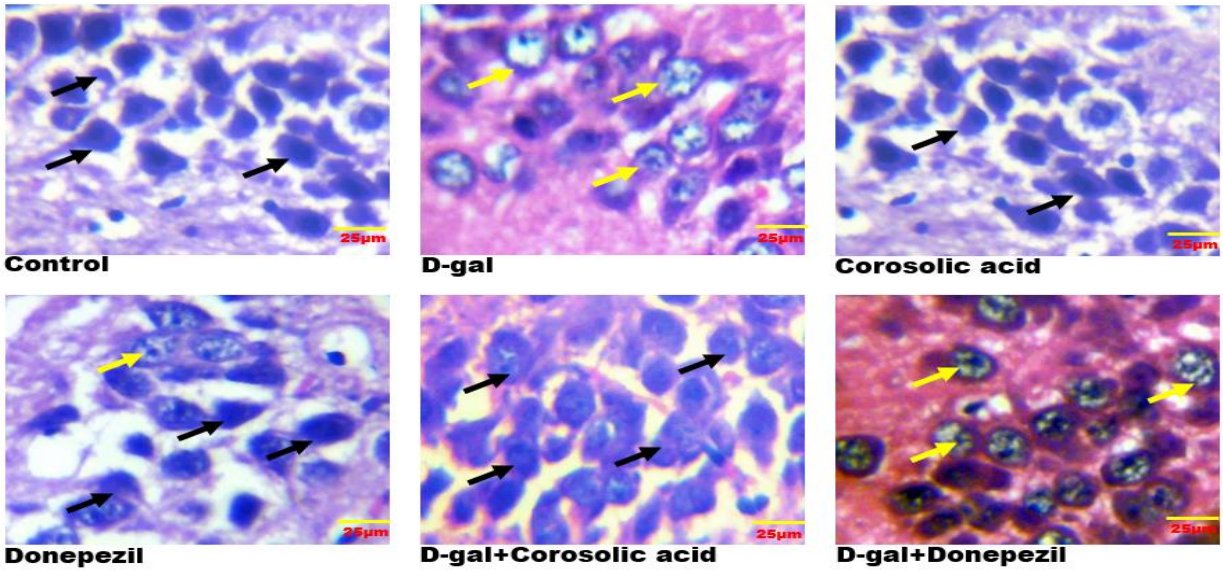

Figure 6: Photomicrographs of the hippocampus stained with Hematoxylin and Eosin (H&E)**.** Scale bar = 25µm. Black arrows show viable pyramidal neurons; yellow arrows indicate shrunken, pyknotic cells. The hippocampal CA3 pyramidal layer is densely populated and orderly in controls, severely depleted and disorganised following D-galactose, and substantially restored by corosolic acid, indicating protection of this selectively vulnerable subfield.

 ISSN: 1595-1693

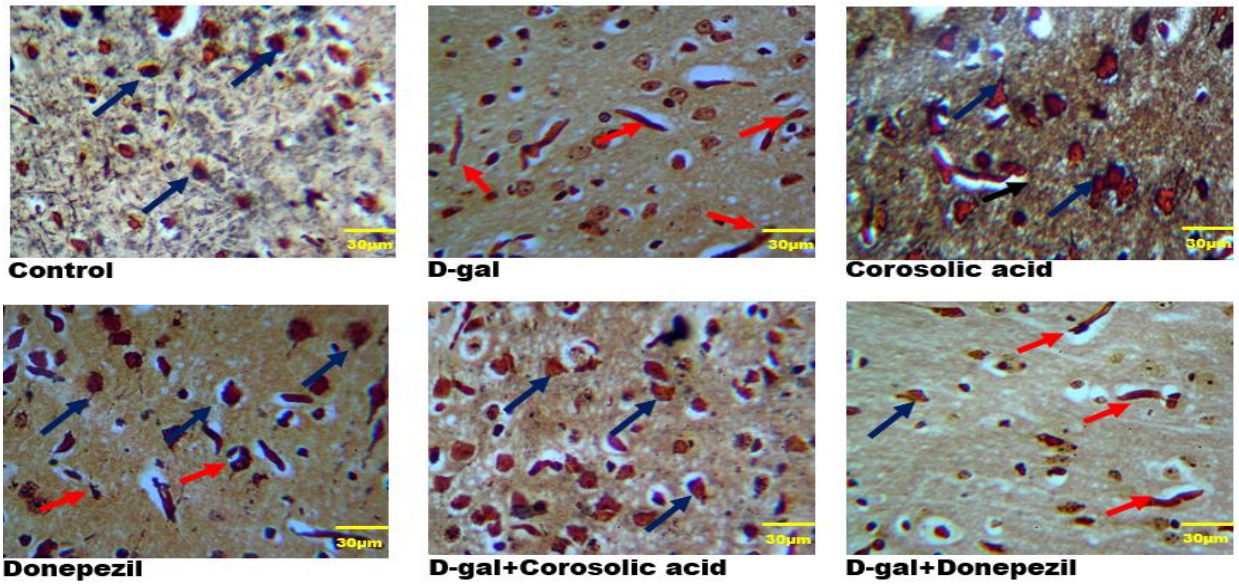

Figure 7: Silver-impregnated histochemical sections of the prefrontal cortex using Bielchowski stain**.** Scale bar = 30µm. Blue arrows show normal neurofibrillary arrangements; red/black arrows highlight neurodegenerative structural changes or axonal fragmentation. Cortical neurofibrils are continuous and well-impregnated in controls, fragmented and tortuous after D-galactose, and largely restored to a continuous pattern by corosolic acid, demonstrating preservation of the neuronal cytoskeleton.

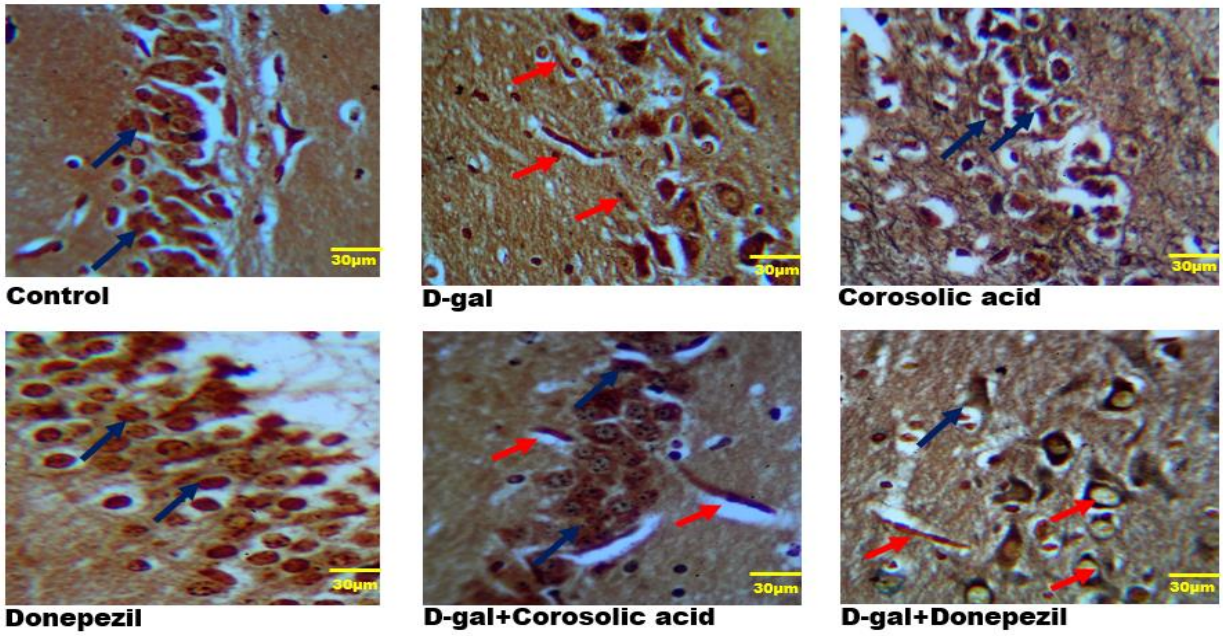

Figure 8: Silver-impregnated histochemical sections of the hippocampus using Bielchowski stain. Scale bar = 30µm. Blue arrows represent intact neurofilaments; red arrows showcase fragmented or aggregated argentophilic structures. Hippocampal silver impregnation shows intact neurofilaments in controls, marked fragmentation and argyrophilic aggregation after D-galactose, and clear preservation of neurofibrillary architecture in the corosolic acid group, paralleling the

 ISSN: 1595-1693

H&E and biochemical results and confirming structural neuroprotection across the corticohippocampal axis.

Histochemical evaluation of the Prefrontal Cortex and Hippocampus (Bielchowski stain)

Control sections displayed well-organised, continuously impregnated neurofibrils in both the prefrontal cortex and hippocampal CA3 (Figures 7 and 8). D-galactose caused neurofibrillary fragmentation, tortuosity and loss of axonal continuity. Corosolic acid markedly preserved neurofibrillary architecture, yielding continuous, well-impregnated fibres, while donepezil showed intermediate protection with scattered fragmented argyrophilic fibres.

Discussion

The present study demonstrates that chronic D-galactose administration produces cognitive, oxidative, neuroinflammatory, cholinergic and structural derangement of the corticohippocampal axis in adult male Wistar rats, and that corosolic acid substantially reverses each of these changes, in several instances to a degree comparable with, or exceeding, the reference cholinesterase inhibitor donepezil. The consistency of the effect across independent behavioural, biochemical and histological readouts strengthens the internal validity of the findings and supports the D-galactose model as a reliable proxy of age-related neurodegeneration (Sadigh-Eteghad et al., 2017; Budni et al., 2016).

D-galactose impaired performance across all three behavioural paradigms — prolonging escape latency in the Morris water maze, reducing spontaneous alternation in the Y-maze, and diminishing novel-object exploration — consistent with the established capacity of chronic D-galactose to induce spatial and recognition memory deficits (Budni et al., 2016). Corosolic acid significantly restored performance on all three tasks, indicating recovery of hippocampal- and prefrontal cortex-dependent cognition. This is in keeping with reports that antioxidant phytochemicals such as caffeine and anthocyanins reverse D-galactose-induced memory impairment (Ullah et al., 2015; Rehman et al., 2017). Notably, corosolic acid restored novel object recognition to near-control levels whereas donepezil did not, suggesting that its behavioural benefit extends beyond cholinergic modulation alone.

At the biochemical level, D-galactose reduced superoxide dismutase activity in both the prefrontal cortex and hippocampus, reflecting depletion of enzymatic antioxidant defence and consequent oxidative stress, a central feature of D-galactose-induced brain ageing (Ionescu-Tucker & Cotman, 2021). Corosolic acid restored SOD activity in both regions — exceeding donepezil in the cortex — consistent with the recovery of antioxidant capacity reported for other plant-derived compounds in this model (Dong et al., 2017; Younis et al., 2024) and with the intrinsic antioxidant activity documented for corosolic acid, which donepezil lacks (Zhao et al., 2021).

D-galactose markedly upregulated NF-κB in the prefrontal cortex and hippocampus, indicating activation of pro-inflammatory transcriptional signalling. Corosolic acid suppressed NF-κB to near-control levels in both regions, comparably with donepezil. This anti-inflammatory action is consistent with evidence that antioxidant phytochemicals attenuate D-galactose-induced neuroinflammation (Chen et al., 2018; Rehman et al., 2017), and specifically with the demonstrated ability of corosolic acid to suppress NF-κB-driven inflammatory mediators in neural tissue (Zhang et al., 2022; Zhao et al., 2021).

A parallel cholinergic disturbance was evident: D-galactose elevated acetylcholinesterase activity in both regions, which would accelerate acetylcholine hydrolysis and compromise cholinergic neurotransmission. Corosolic acid normalised AChE activity toward control values, an effect comparable with that of donepezil in the hippocampus. A reduction in AChE following phytochemical treatment has similarly been

 ISSN: 1595-1693

reported in D-galactose-based models (Haider et al., 2020); that corosolic acid, without being a designed cholinesterase inhibitor, lowered AChE to the same extent as donepezil is consistent with an indirect benefit arising from reduced oxidative and inflammatory injury to cholinergic neurons.

The histological and histochemical findings provide structural corroboration of the biochemical and behavioural data. H&E staining revealed D-galactose-induced neuronal degeneration — shrinkage, cytoplasmic vacuolation and nuclear pyknosis — in the prefrontal cortex and hippocampal CA3, a region recognised as selectively vulnerable to oxidative and inflammatory insult (Olajide et al., 2021). Bielschowsky silver impregnation further demonstrated fragmentation and discontinuity of neurofibrils in the D-galactose group. Corosolic acid preserved both neuronal morphology and neurofibrillary continuity, exceeding the partial protection seen with donepezil, thereby linking the functional recovery to genuine preservation of corticohippocampal structural integrity.

The molecular pathways mediating these effects are probably worthwhile targets for further scrutiny. First, the recovery of superoxide dismutase activity indicates the activation of the Keap1–Nrf2–ARE pathway, the master regulator of the cellular antioxidant response. Under basal conditions, Nrf2 is sequestered in the cytoplasm by Keap1 and targeted for degradation. Oxidative or electrophilic stress results in release of Nrf2, which translocates to the nucleus and drives transcription of antioxidant-response-element genes, including those encoding superoxide dismutase, catalase, and the glutathione system. Pentacyclic triterpenoids structurally related to corosolic acid are known Nrf2 activators, and other phytochemicals rescue the D-galactose phenotype specifically through this axis (Dong et al., 2017). The recovery of SOD observed here is therefore most parsimoniously attributed to Nrf2 activation. Second, NF-κB inhibition signals a direct impact on inflammatory transcription. NF-κB is the major transcription factor that drives microglial production of pro-inflammatory mediators in the ageing brain and its inhibition would diminish the cytokine burden that promotes synaptic and neuronal injury. Third, these two pathways are mechanistically coupled, and this coupling helps explain the magnitude of protection observed. Reactive oxygen species are themselves potent activators of NF-κB and vice versa, since NF-κB-driven inflammatory enzymes produce further oxidative species. The Keap1–Nrf2 and NF-κB systems are thus reciprocally antagonistic, in which the antioxidant arm is strengthened at the expense of the inflammatory arm and vice versa. The simultaneous restoration of SOD and inhibition of NF-κB would break a self-amplifying oxidative–inflammatory loop, in keeping with the coordinated normalisation of both markers here and the coupled antioxidant and anti-inflammatory actions reported for the compound in non-neural tissue (Zhao et al., 2021).

Fourth, a mechanistic comment can be made on the cholinergic effect. Corosolic acid is not a rationally designed acetylcholinesterase inhibitor, but it normalised AChE activity to a similar extent as donepezil. Two non-mutually exclusive explanations are possible: a direct, weak inhibitory interaction with the enzyme, and – more likely given the profile of the compound – an indirect effect whereby reduced oxidative and inflammatory injury to cholinergic neurons lowers the compensatory up-regulation of AChE that accompanies cholinergic stress. In contrast to single-target reference drugs, phytochemicals are characterised by multi-target pharmacology, with convergence of antioxidant, anti-inflammatory, and cholinergic actions on a single tissue.

Limitations of the Study

The limitations of the present study should be acknowledged so that the findings may be interpreted in proper perspective. The work was done only in adult male Wistar rats. There are large sex differences in oxidative, inflammatory and hormonal responses; thus, the results cannot be extrapolated to females without direct testing. Inter-strain and inter-individual variability

 ISSN: 1595-1693

inherent to rodent models may limit reproducibility across laboratories.

Future Directions and Clinical Perspectives

These limitations define a clear programme of future work. Direct interrogation of the proposed mechanism is the immediate priority: immunohistochemical and Western blot quantification of nuclear Nrf2, Keap1, downstream antioxidant enzymes, and NF-κB phosphorylation would confirm the pathway inferred here, while a dose–response design would establish the minimum effective dose and therapeutic window. Furthermore, because the D-galactose paradigm models the oxidative and inflammatory features of brain ageing rather than the full amyloid–tau pathology of Alzheimer's disease, confirmation in transgenic amyloid or tau models, and ultimately in early-phase human studies, would be necessary before clinical claims could be made. Corosolic acid nonetheless emerges from this work as a promising, inexpensive and orally available candidate that merits this further investigation.

Conclusion

Corosolic acid attenuated D-galactose-induced cognitive impairment, restored superoxide dismutase activity, suppressed NF-κB, normalised acetylcholinesterase activity, and preserved neuronal and neurofibrillary architecture within the prefrontal cortex and hippocampus. Its efficacy was comparable or superior to donepezil on several endpoints, indicating that corosolic acid exerts multi-target neuroprotection and merits further mechanistic and translational investigation in age-related neurodegeneration.

Professional and Translational Implications

This study and its direct findings have some professional and translational implications. "For the neuroscience and pharmacology community, it broadens the known metabolic and oncological pharmacology of corosolic acid to neuroprotection, identifying the corticohippocampal axis as a responsive target and providing a rationale for mechanistic follow-up." In drug-discovery efforts for dementia, the demonstration that an inexpensive, orally active and already-marketed dietary triterpenoid can match a licensed cholinesterase inhibitor across multiple endpoints supports the repurposing of nutraceutical compounds as adjuncts or leads in age-related cognitive decline. This is of particular relevance for clinical and public-health practitioners in low- and middle-income settings, where the burden of dementia is greatest and access to disease-modifying therapy is most limited. The findings also highlight the importance of multi-target agents for both researchers and regulators in a disease that has proven resistant to single-target strategies.

Conflict of Interest

The authors declare that they have no known competing financial interests or personal relationships that could have appeared to influence the work reported in this paper.

Funding

This research did not receive any specific grant from funding agencies in the public, commercial, or not-for-profit sectors.

Acknowledgements

The authors gratefully acknowledge the technical staff of the Department of Anatomy, Faculty of Basic Medical Sciences, Osun State University, for their assistance with animal husbandry, histological processing and biochemical assays.

References

Beshir, S. A., Hussain, N., Menon, V. B., Al Haddad, A. H. I., Al Hemyari, S. S., & Elnour, A. A. (2024). Advancements and challenges in antiamyloid therapy for Alzheimer's disease: A comprehensive review. *International Journal of Alzheimer's Disease, 2024*, 2052142. https://doi.org/10.1155/2024/2052142

Breijyeh, Z., & Karaman, R. (2020). Comprehensive review on Alzheimer's

disease: Causes and treatment. *Molecules, 25*(24), 5789. https://doi.org/10.3390/molecules25245789

Budni, J., Pacheco, R., da Silva, S., Garcez, M. L., Mina, F., Bellettini-Santos, T., … Quevedo, J. (2016). Oral administration of D-galactose induces cognitive impairments and oxidative damage in rats. *Behavioural Brain Research, 302*, 35–43. https://doi.org/10.1016/j.bbr.2015.12.041 [APA-7: list all authors (≤20) and replace the ellipsis with the full author list.]

Chen, P., Chen, F., & Zhou, B. (2018). Antioxidative, anti-inflammatory and anti-apoptotic effects of ellagic acid in D-galactose-induced aging in mice. *Scientific Reports, 8*, 1465. https://doi.org/10.1038/s41598-018-19732-0

Deng, S., Lu, H., Chi, H., Wang, Y., Li, X., & Ye, H. (2020). Neuroprotective effects of OMO within the hippocampus and cortex in a D-galactose and $A\beta_{25–35}$-induced rat model of Alzheimer's disease. *Evidence-Based Complementary and Alternative Medicine, 2020*, 1067541. https://doi.org/10.1155/2020/1067541

d'Errico, P., & Meyer-Luehmann, M. (2020). Mechanisms of pathogenic tau and Aβ protein spreading in Alzheimer's disease. *Frontiers in Aging Neuroscience, 12*, 265. https://doi.org/10.3389/fnagi.2020.00265

Dong, F., Wang, S., Wang, Y., Yang, X., Jiang, J., Wu, D., Qu, X., Fan, H., & Yao, R. (2017). Quercetin ameliorates learning and memory via the Nrf2-ARE signalling pathway in D-galactose-induced neurotoxicity in mice. *Biochemical and Biophysical Research Communications, 491*(3), 636–641. https://doi.org/10.1016/j.bbrc.2017.07.151

GBD 2019 Dementia Forecasting Collaborators. (2022). Estimation of the global prevalence of dementia in 2019 and forecasted prevalence in 2050: An analysis for the Global Burden of Disease Study 2019. *The Lancet Public Health, 7*(2), e105–e125. https://doi.org/10.1016/S2468-2667(21)00249-8

Haider, S., Liaquat, L., Ahmad, S., Batool, Z., Siddiqui, R. A., Tabassum, S., Shahzad, S., Rafiq, S., & Naz, N. (2020). Naringenin protects $AlCl_3$/D-galactose induced neurotoxicity in rat model of AD via attenuation of acetylcholinesterase levels and inhibition of oxidative stress. *PLOS ONE, 15*(1), e0227631. https://doi.org/10.1371/journal.pone.0227631

Ionescu-Tucker, A., & Cotman, C. W. (2021). Emerging roles of oxidative stress in brain aging and Alzheimer's disease. *Neurobiology of Aging, 107*, 86–95. https://doi.org/10.1016/j.neurobiolaging.2021.07.014

Kraeuter, A.-K., Guest, P. C., & Sarnyai, Z. (2019). The Y-maze for assessment of spatial working and reference memory in mice. In P. C. Guest (Ed.), *Pre-clinical models: Techniques and protocols* (Methods in Molecular Biology, Vol. 1916, pp. 105–111). Humana Press. https://doi.org/10.1007/978-1-4939-8994-2_10

Olajide, O. J., Suvanto, M. E., & Chapman, C. A. (2021). Molecular mechanisms of neurodegeneration in the entorhinal cortex that underlie its selective vulnerability during the pathogenesis of Alzheimer's disease. *Biology Open, 10*(1), bio056796. https://doi.org/10.1242/bio.056796

Rehman, S. U., Shah, S. A., Ali, T., Chung, J. I., & Kim, M. O. (2017). Anthocyanins reverse D-galactose-induced oxidative stress and neuroinflammation-mediated cognitive impairment in adult rat brain. *Molecular Neurobiology, 54*(1), 255–271. https://doi.org/10.1007/s12035-015-9604-5

Sadigh-Eteghad, S., Majdi, A., McCann, S. K., Mahmoudi, J., Vafaee, M. S., & Macleod, M. R. (2017). D-galactose-induced brain ageing model: A systematic review and meta-analysis on cognitive outcomes and oxidative stress indices. *PLOS ONE, 12*(8), e0184122.

https://doi.org/10.1371/journal.pone.0184122

Scheltens, P., De Strooper, B., Kivipelto, M., Holstege, H., Chételat, G., Teunissen, C. E., Cummings, J., & van der Flier, W. M. (2021). Alzheimer's disease. *The Lancet, 397*(10284), 1577–1590. https://doi.org/10.1016/S0140-6736(20)32205-4

Sexton, C., Snyder, H. M., Chandrasekaran, L., Worley, S., & Carrillo, M. C. (2021). Expanding representation of low and middle income countries in global dementia research: Commentary from the Alzheimer's Association. *Frontiers in Neurology, 12*, 633777. https://doi.org/10.3389/fneur.2021.633777

Tropea, M. R., Sanfilippo, G., Giannino, F., Davì, V., Gulisano, W., & Puzzo, D. (2022). Innate preferences affect results of object recognition task in wild type and Alzheimer's disease mouse models. *Journal of Alzheimer's Disease, 85*(4), 1343–1356. https://doi.org/10.3233/JAD-215209

Ullah, F., Ali, T., Ullah, N., & Kim, M. O. (2015). Caffeine prevents D-galactose-induced cognitive deficits, oxidative stress, neuroinflammation and neurodegeneration in the adult rat brain. *Neurochemistry International, 90*, 114–124. https://doi.org/10.1016/j.neuint.2015.07.001

Wang, X., Fu, X., Luo, X., Lai, Y., Cai, C., Liao, Y., Dai, Z., Fang, S., & Fang, J. (2023). Network proximity analysis deciphers the pharmacological mechanism of osthole against D-galactose-induced cognitive disorder in rats. *Molecules, 29*(1), 21. https://doi.org/10.3390/molecules29010021

Younis, R. L., El-Gohary, R. M., Ghalwash, A. A., Hegab, I. I., Ghabrial, M. M., Aboalsoud, A., … El-Azzem, A. A. (2024). Luteolin mitigates D-galactose-induced brain ageing in rats: SIRT1-mediated neuroprotection. *Neurochemical Research, 49*, 2803–2820. https://doi.org/10.1007/s11064-024-04203-y

[APA-7: list all authors (≤20) and replace the ellipsis with the full author list.]

Zeng, L., Lin, L., Chen, L., Xiao, W., & Gong, Z. (2021). L-Theanine ameliorates D-galactose-induced brain damage in rats via inhibiting AGE formation and regulating sirtuin1 and BDNF signalling pathways. *Oxidative Medicine and Cellular Longevity, 2021*, 8850112. https://doi.org/10.1155/2021/8850112

Zhang, L., Sui, S., Wang, S., & Sun, J. (2022). Neuroprotective effect of corosolic acid against cerebral ischemia-reperfusion injury in experimental rats. *Journal of Oleo Science, 71*(10), 1501–1510. https://doi.org/10.5650/jos.ess22130

Zhao, J., Zhou, H., An, Y., Shen, K., & Yu, L. (2021). Biological effects of corosolic acid as an anti-inflammatory, anti-metabolic syndrome and anti-neoplasic natural compound (Review). *Oncology Letters, 21*(2), 84. https://doi.org/10.3892/ol.2020.12345

Citation*:*
Adunfe, O. O., Abayomi, T. A., Tokunbo, O. S., Olayemi, O. S., Oguntade, A. A., Farinde, R. A., Oyadare, O. S., & Dare, B. J. (2026). Corosolic Acid Attenuates Cognitive Deficits, Oxidative Stress, Neuroinflammation and Corticohippocampal Neurodegeneration in D-galactose-Induced Alzheimer's Disease in Adult Wistar Rats. *Fountain Journal of Basic Medical and Health Sciences (FUJBMHES), 2(1),* 122-139.